PAPER

NJC
www.rsc.org/njc

Shaping zirconium phosphate α-$Zr(HPO_4)_2 \cdot H_2O$: from exfoliation to first α-ZrP 3D open-cell macrocellular foams

Florent Carn,[a] Alain Derré,[a] Wilfrid Neri,[a] Odile Babot,[b] Hervé Deleuze[b] and Rénal Backov*[a]

[a] *Centre de Recherche Paul Pascal, CRPP UPR CNRS 8641, 115 avenue Albert Schweitzer, 33600 PESSAC, France. E-mail: backov@crpp-bordeaux.cnrs.fr; Fax: 33(0)5 56 84 56 00; Tel: 33(0)5 56 84 56 30*

[b] *Laboratoire de Chimie Organique et Organométallique, UMR 5802-CNRS, Université Bordeaux 1, 351 Cours de la Libération, 33045 Talence Cedex, France*

Received (in Montpellier, France) 2nd June 2005, Accepted 20th July 2005
First published as an Advance Article on the web 4th August 2005

Using a two-step synthetic route that first takes benefit of an α-$Zr(HPO_4)_2 \cdot H_2O$ (α-ZrP) exfoliation process followed by an air–liquid foam shaping method we have designed for the first time 3D macrocellular foams made of α-ZrP lamellae. Apart from this high scale texturation we were able to tune the macroscopic void space shapes (polygonal-type or spherical-type) as well as cell wall thickness by varying the starting foam's water volume fraction (ρ). Also, by adjusting the size of the porous disk employed during the bubbling process we can define the macroscopic cell diameters with a strong degree of control.

Introduction

Chemistry of shapes is a new domain of research that encompasses the areas of chemistry, physical-chemistry and of biology.[1] By combining soft chemistry and fluid complexes[2] it is possible to promote architectures hierarchically organized leading to the concept of "synthesis over all length scale".[3] In this specific context, sol–gel chemistry and lyotropic mesophases can be associated to generate inorganic polymers with mesoscopic void spaces while metastable thermodynamic systems can induce macroscopic organization.[2,4] For instance, mesoporous silica hollow spheres can be reached using either direct[5] or reverse emulsion[6] to pattern these specific shapes. For example, by employing a direct emulsion it is possible to reach macrocellular silica[2] or titanium oxide monoliths.[7] In this connection, we were able for the first time to tune the macroscopic cell diameters of such monoliths by increasing the oil volume fraction of the starting emulsion, leading to enhancement of both the emulsion viscosity and the shearing effect applied over the droplets, so minimizing their diameters.[4] In order to increase the size of the macroscopic cells above 70 μm we have to switch toward another metastable thermodynamic system, namely air–liquid foams. By combining the sol–gel process and air–liquid foams as a macroscopic template we obtained diverse inorganic macrocellular foams where both the macroscopic cell shapes and diameters as well as the cell wall (called in rheology the Plateau-border) thicknesses were designed with a strong degree of control.[8–10] This approach should certainly not be restricted to inorganic oxide polymers. We decided to extend the approach to the mineral salt zirconium bis(monohydrogen orthophosphate) monohydrate, $Zr(HPO_4)_2 \cdot H_2O$ (α-ZrP). The α-ZrP structure is layered[11] and exhibits ion-sieve and enhanced catalytic properties,[12] especially due to the presence of acid P–OH groups on the surfaces.[11,13] A wide scope of guest entities have been intercalated into the α-ZrP lamellae, ranging from luminescent cations,[14] organic molecules with diverse properties (optical, conductivity and so forth)[15] to protein macromolecules[16] or polymers.[17] Also, besides possible application in chemical processing of radioactive materials, new insights have been recently found toward water desalination and fuel cells.[18] In order to access phase separations associated with catalysis or filtration-ion exchange applications, the generation of interconnected mesoporous–macroporous monolith-type materials appears an important task—as seen from the increase of research dedicated to inorganic aerogels.[19] Also, despite the confinement media that offers an α-ZrP interlayer gallery, a major problem is that expansion of the host sheets and inward diffusion of the guest entities during the intercalation processes constitute enthalpy penalties leading for instance to a concentration threshold in the binding isotherm of analyte molecules.[20] This characteristic limits in all cases the cation exchange kinetics, and monophasic configuration of the guest organic entities through the entire interlayer galleries is not assured. One possible answer is to exfoliate the sheets, a strategy widely used to promote supramolecular assemblies,[21] thin self-standing films[22] or membranes.[23]

We describe herein the first three-dimensional shaping of α-ZrP using an air–liquid foam macroscopic pattern and a widely used unilamellar colloid of α-ZrP produced through exfoliation of the lamellae with methylamine.[24] We demonstrate the capability of obtaining zirconium phosphate macrocellular foams where both the shape and thickness of the macroscopic cells and walls can be tuned upon varying the starting foam's water volume fraction, while macroscopic cell diameters are a function of the capillary sizes used during the bubbling process.

Experimental

Materials

All materials were used as received without further purification. Zirconium tetraethoxide and Tergitol NP9 were purchased from Aldrich. Orthophosphoric acid (85%) and fluoridric acid (40%) were purchased from Prolabo.

DOI: 10.1039/b507960h

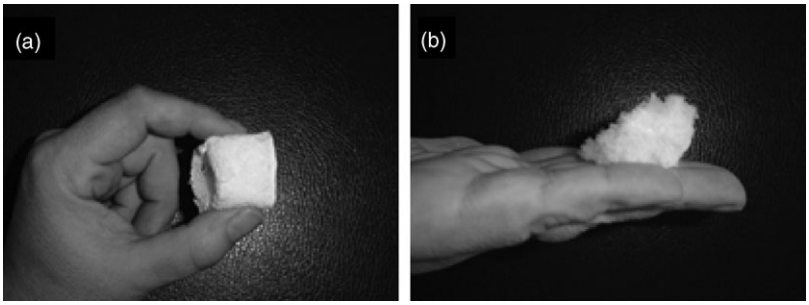

Fig. 1 Zirconium phosphate hybrid foams obtained as a monolith. a) Monolith obtained with a bubbling apparatus pore size range of 16–40 μm, b) monolith obtained with a bubbling apparatus pore size of 40–100 μm.

Synthesis

The synthesis of α-ZrP for this study is directly taken from ZrF_6^{2-} metathetic decomplexation under phosphoric acid conditions.[25] 7 g of zirconium tetraethoxide is dispersed within 150 ml of deionised water and 84 ml of H_3PO_4 is added. The solution is stirred for two hours in order to promote both zirconium tetraethoxide hydrolysis and concomitant amorphous zirconium phosphate precipitation. Then 4 ml of HF are added to this solution placed within a plastic canister and the solution is stirred until completely clear. This solution is allowed to evaporate at 70 °C while the volume is kept constant by addition of deionised water. Finally α-ZrP microcrystals are washed three times with deionised water and allowed to dry in air. Then 3.7 g of α-ZrP is dispersed within 170 ml of deionised water and 1.2 g of methylamine is added drop by drop. The total volume is then brought to 200 ml by adding deionised water and the appearing gel is then sonicated for one hour, stirred over night and allowed to age for four days. Finally, 2.1 g of Tergitol NP9 is added and the resulting mixture is stirred for one hour. During this period the gel viscosity decreases. This neutral surfactant was chosen both to stabilize the foams during the bubbling process and to avoid α-ZrP flocculation. The as-synthesized sol is very stable, even over a period of two months, meaning that α-ZrP does not flocculate (individual sheets do not stack on each other).

Foaming process

The air–liquid bubbling processes start in a plexiglas column (2.5 cm × 2.5 cm × 60 cm high) under a specific sol flux, (Q) that allows wetting of the growing foams. Foam was obtained by bubbling perfluorohexane saturated with nitrogen through a porous glass disk (porosity: 100–160 μm, 40–100 μm, 16–40 μm) into the foaming solution. The metastable foams were collected at the top of the column with a spatula and placed in a beaker. These foams were then frozen over night at −80 °C and lyophilised for 5 h. The resulting hybrid organic–inorganic monolith-type materials were then heated at 400 °C in air to both calcine the surfactant and sinter the inorganic scaffolds. For the calcinations, the increase of temperature was monitored at 2 °C min^{-1} with a first plateau at 200 °C for 2 h. The cooling process was uncontrolled and directed by the oven inertia.

Characterization

SEM observations were performed with a JEOL JSM-5200 scanning electron microscope operating at 25 kV. The specimens were gold-coated prior to examination. TEM experiments were performed with a Jeol 2000 FX microscope (accelerating voltage of 200 kV). The samples were prepared as follows: powdered zirconium phosphate foams were deposited on a copper grid coated with a formvar membrane. XRD measurements were obtained using an X'pert MPD Philips using Cu Kα radiation with an average current of 50 mA. Thermogravimetric analyses (TGA) were carried out under an oxygen flux (5 cm^3 min^{-1}) using a heating rate of 5 °C min^{-1}. The apparatus is a Stearam TAG-1750 thermo gravimetric analyser.

Results and discussion

Upon the two-step exfoliation–foaming strategy described above, the final zirconium phosphate compounds appear in a three-dimensional monolith state (Fig. 1).

It is well known that a colloid of α-ZrP, made of exfoliated sheets, has the capability of forming self-standing films upon drying, mainly induced by the enhanced anisotropic aspect ratio of the α-ZrP particles.[24,25] Herein we associate to the exfoliation process a metastable thermodynamic system, namely air–liquid foams, to promote a template at the macroscopic length scale thus offering for the first time the capability of generating zirconium phosphate macrocellular foams. The overall strategy is summarized in Scheme 1.

By extending a non-static foaming pattern method[8–10] to α-ZrP we first aim to tune the macroscopic cell morphologies by adjusting the starting air–liquid foam liquid fractions (ρ); knowing that ρ corresponds to the volume of liquid constituting the foam divided by the foam total volume. The relationship between ρ and the foam morphology can be expressed with the following equation:[26]

$$\rho = 0.171(r/L_{PB})^2 + 0.256(r/L_{PB})^3 \approx a/L_{PB}{}^{2*}\,[1 + 3.98(a/L_{PB}{}^2)^{1/2}]$$

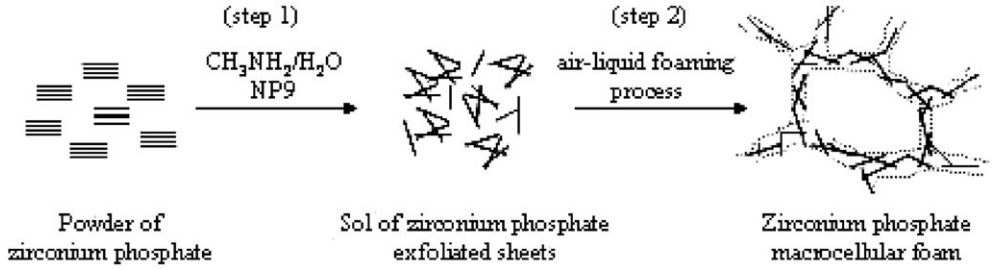

Scheme 1 General two-step procedure used to promote zirconium phosphate macrocellular foams.

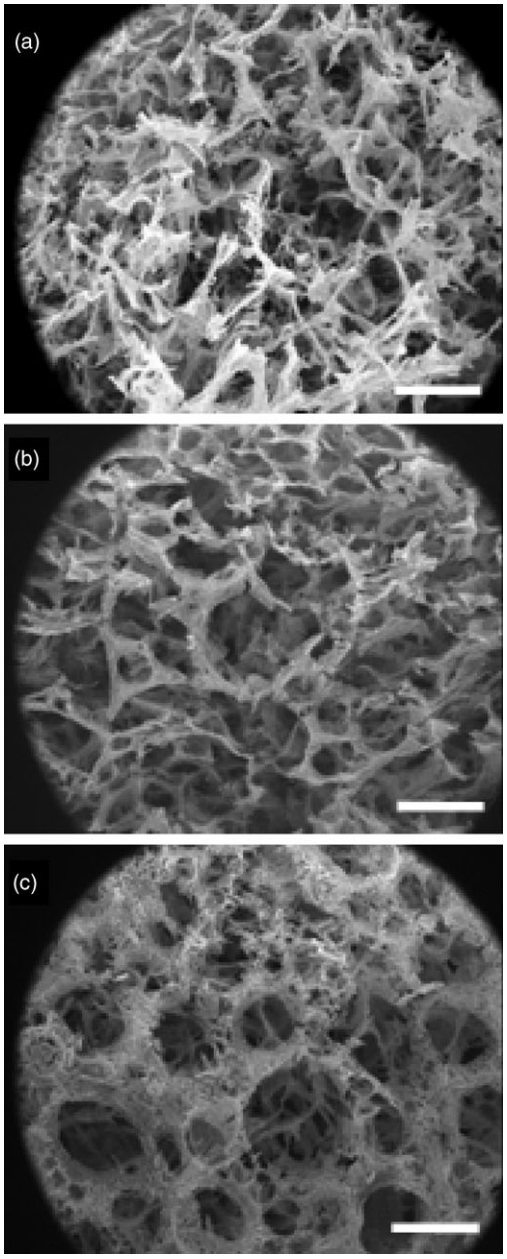

Fig. 2 SEM pictures of zirconium phosphate hybrid foams obtained by varying the sol flux (Q) imposed at the top of the foam during the bubbling process. a) $Q = 0$ g s^{-1} (foams not wet from above), b) $Q = 0.12$ g s^{-1}, c) $Q = 0.22$ g s^{-1}. The scale bars represent 600 μm.

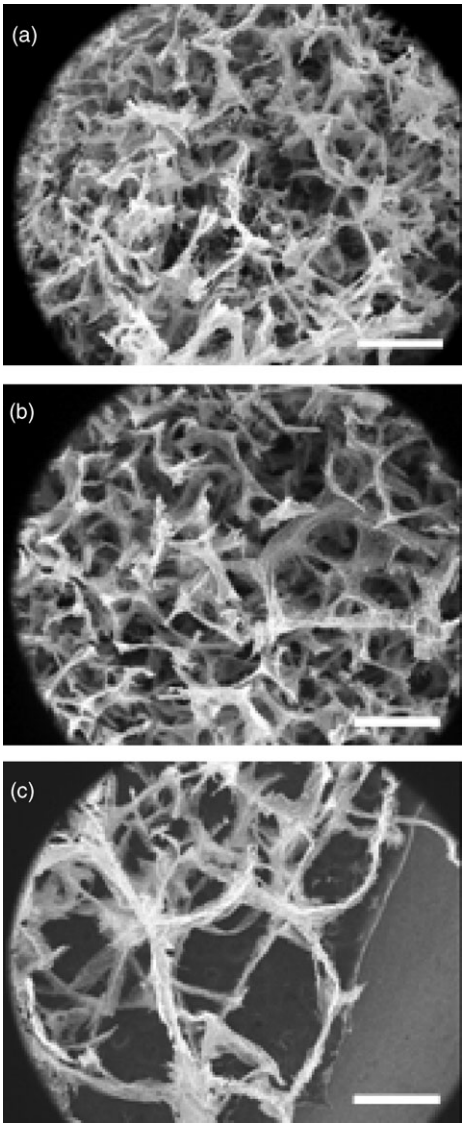

Fig. 3 SEM pictures of the zirconium phosphate hybrid foams obtained with different pore size apparatus at a constant sol flux ($Q = 0$ g s^{-1}). a) Pore size range 16–40 μm, b) pore size range 40–100 μm, c) pore size range 100–160 μm. The scale bars represent 600 μm.

Where "r" is the Plateau border (rheology terminology for the cell walls) curvature, "L_{PB}" is the Plateau border length and "a" is the Plateau border width. The foam liquid fraction can be tuned by varying the sol flux (Q) injected at the top of the foam. Using this drainage property either polygonal-type (Fig. 2a and 2b) or more spherical-type (Fig. 2c) α-ZrP macroscopic cell morphologies are obtained. Beyond the inorganic scaffold macrocellular shapes, the cell wall thicknesses can be tuned by varying the foam's liquid fraction. In this connection, α-ZrP cell wall thicknesses are strongly related to the wetting strength (Q) applied at the top of the starting air–liquid foams (Fig. 2).

In order to modulate the average macroscopic cell diameters we varied the porous disk employed at the bottom of the column during the bubbling process (Fig. 3). We can observe that the Plateau border lengths can vary from around 100 μm up to more than 600 μm. In regards to the SEM pictures (Fig. 3), we can notice a polydispersity associated to the cell diameter. This polydisperse nature is first induced by the pore sizes of the bubbling apparatus, which are associated to a pore size range, 16–40 μm for instance, and not to a single pore size value. Secondly, this polydispersity is enhanced by an intrinsic thermodynamic phenomenon that is well-known to be a strong penalty toward bubble size monodispersity, namely the Oswald ripening.[27]

Also, whatever the experimental condition in use, SEM investigation of the foam wall reveals a secondary intra-wall macroporosity (Fig. 4a). This secondary porosity is certainly caused *via* the statistical aggregation of the particles during the sublimation process. Also, we can notice that the aspect ratio of the particles, that constitute the foam walls, is high with a very thin sheet-like topology (Fig. 4b).

TGA experiments have been performed in air in order to determine the hybrid foam stoichiometry (Fig. 5).

The total weight loss associated to α-ZrP, from ambient temperature and up to 550 °C, is 12% which corresponds to the loss of two water molecules leading to the formation of pyrophosphate ZrP_2O_7 (Fig. 5a).[11] Over the same temperature range the total weight loss of the powder, resulting from the drying of α-ZrP/methylamine exfoliated colloid, is 20% (Fig. 5b). When compared with the weight loss associated to α-ZrP for the same temperature range the amount of organic matter coming from the methylamine is 8% which corresponds to the

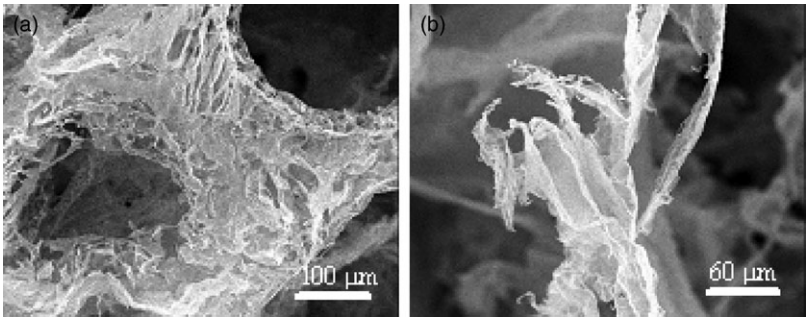

Fig. 4 SEM visualization of the zirconium phosphate hybrid foam wall obtain with the pore sizes range (16–40 μm) at a constant sol flux ($Q = 0$ g s^{-1}), b) same sample at different magnification.

following stoichiometry, $Zr(HPO_4)_2(CH_3NH_2)_{0.85} \cdot 1H_2O$. Finally, taking into account the previous result and the total weight loss of 69% associated to the hybrid foams (Fig. 5c) the amount of organic matter associated to the tergitol NP9 ($C_{33}O_{10}H_{60}$) is 49% which corresponds to the following stoichiometry of the hybrid zirconium phosphate foams obtained through this study, $Zr(HPO_4)_2(CH_3NH_2)_{0.85} \cdot 1H_2O/(C_{33}O_{10}H_{60})_{0.54}$. We can observed that the organic weight loss associated to the hybrid foams is completed at 350 °C, which is the main reason why the temperature treatment of the hybrid foam was chosen to be 400 °C for 6 hours in air. Also, by increasing the temperature treatment up to 650 °C, final pyrophosphate scaffolds do not collapse. The second reason why we choose to stop the calcination temperature at 400 °C is because it has been recently proven that α-ZrP enhances acid, basic or redox sites when treated at 300 °C, properties that decrease slightly when treated at 500 °C where zirconium pyrophosphate (ZrP_2O_7) is obtained.[18]

In order to assess the microstructure of the zirconium phosphate compounds we performed XRD experiments (Fig. 6). First the synthetic procedure employed for this study allows reaching well crystalline α-ZrP with specific d_{001} interlayer distance of 7.56 Å (Fig. 6a). Following dispersal of α-ZrP in water and exfoliation using methylamine the XRD pattern reveals an amorphous character where all the 00l diffraction lattices have vanished, meaning both that the layered compound is in fact exfoliated and that the sheets are subject to partial hydrolysis (Fig. 6, inset).[24,25] When tergitol is added to the previous colloidal sol we notice that the XRD pattern is still the same (Fig. 6, inset), a feature that demonstrates that this non-ionic surfactant is not promoting flocculation of the α-ZrP sheets. Also we can observe on Fig. 6 that the XRD patterns performed on $Zr(HPO_4)_2(CH_3NH_2)_{0.85} \cdot 1H_2O$ self-standing film, powdered to avoid preferential orientation (Fig. 6b), and $Zr(HPO_4)_2(CH_3NH_2)_{0.85} \cdot 1H_2O/(C_{33}O_{10}H_{60})_{0.54}$ hybrid foam (Fig. 6c) are rather similar, thus enhancing the fact that the tergitol entities are not interacting with the zirconium phosphate sheets. In both case we obtained a

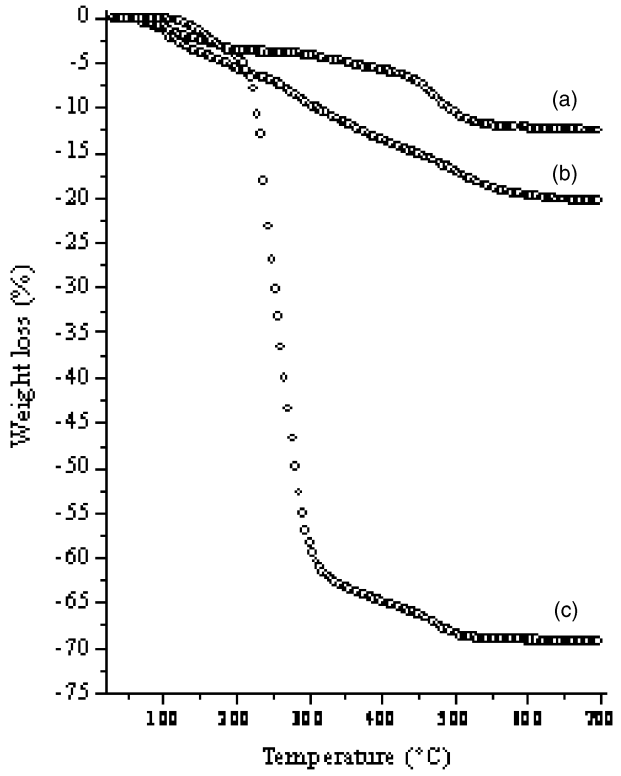

Fig. 5 TGA experiments performed in air with a heating rate of 2 °C min^{-1}. a) α-ZrP, b) α-ZrP/methylamine exfoliated colloid, c) hybrid α-ZrP macrocellular foam.

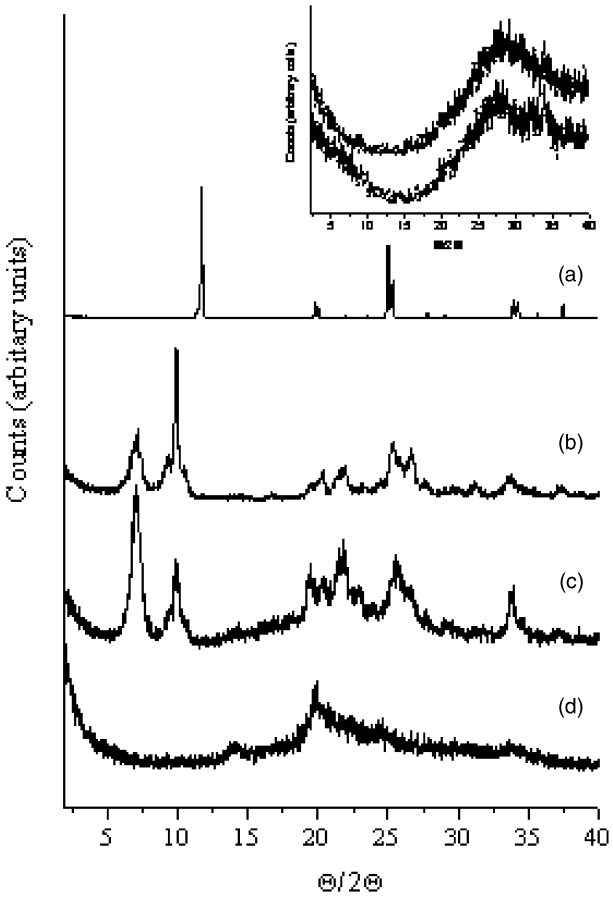

Fig. 6 XRD patterns of: a) α-ZrP, b) $Zr(HPO_4)_2(CH_3NH_2)_{0.85} \cdot 1H_2O$ powdered self-standing film, c) $Zr(HPO_4)_2(CH_3NH_2)_{0.85} \cdot 1H_2O/(C_{33}O_{10}H_{60})_{0.54}$ hybrid foam, d) zirconium phosphate foam treated at 400 °C. Inset: (+, bottom) α-ZrP/methylamine colloidal sol, (○, top) α-ZrP/methylamine/tergitol colloidal sol.

biphasic system with two sets of interlayer distances d^1_{002} and d^2_{002} of respectively 12.4 Å and 10.0 Å.

The biphasic nature of these phases can be explained by the fact that, beyond exfoliation, the methylamine molecules are promoting partial hydrolysis of zirconium phosphate lamellae, thus enhancing their mechanical flexibility and so their ability to accommodate diverse amounts and/or configurations of the intercalated guests.[20,24]

At first glance, the fact that both $Zr(HPO_4)_2(CH_3NH_2)_{0.85} \cdot 1H_2O$ powdered self-standing film and $Zr(HPO_4)_2(CH_3NH_2)_{0.85} \cdot 1H_2O/(C_{33}O_{10}H_{60})_{0.54}$ depict the same biphasic nature with moreover the same interlayer distances, is not obviously explicable, mainly because the drying process for those two set of compounds are not the same at all. In the $Zr(HPO_4)_2(CH_3NH_2)_{0.85} \cdot 1H_2O$ former case the compound is allowed to dry in air thus favoring lamellae self-stacking (flocculation) upon the water evaporation process. This is not the case for the hybrid foams where the driving force associated to the cold-lyophilisation drying process is not water evaporation but rather sublimation. To explain the *d* spacing similitude, despite the discrepancy of the drying processes that have been used, we can hypothesize the following scenario. Specific parallel configuration of the anisotropic exfoliated lamellae within the Plateau-borders of the starting air–liquid foams is certainly enhanced by the high sol flux existing in this specific region of the foam.[26] The sol flux that exists within the Plateau-borders regions is aligning, by a shear stress effect, the zirconium phosphate sheets parallel to each other due to their high aspect ratio. By heating the hybrid foams up to 400 °C we can observe that despite the enhanced amorphous character of the zirconium phosphate foams (Fig. 6d), a d_{002} spacing of 6.4 Å is preserved, a distance that corresponds to the α-ZrP sheet thickness.[11] Also the allotropic transformation toward pyrophosphate ZrP_2O_7 is not yet completed.

Conclusion

Upon a non static patterning method that combines α-ZrP colloid exfoliated sheets and an air–liquid foaming process zirconium phosphate macrocelluar foams have been obtained. At the macroscopic length scale we designed both the cell shapes and wall thickness while the cell diameters varied with the size of the capillary used during the bubbling process. The macrocellular foams reveal sub-macroporosity of the intra-walls. These macrocellular foams made of α-ZrP exfoliated sheets and obtained within a monolith state should enhance the applications associated to zirconium phosphate.

References

1 S. Mann, *Nature*, 1993, **365**, 499.
2 A. Imhof and D. J. Pine, *Nature*, 1997, **389**, 948.
3 I. Soten and G. A. Ozin, *Curr. Opin. Colloid Interface Sci.*, 1999, **4**, 325.
4 F. Carn, A. Colin, M.-F. Achard, E. Sellier, M. Birot, H. Deleuze and R. Backov, *J. Mater. Chem.*, 2004, **14**, 1370.
5 S. Schacht, Q. Huo, I. G. Voigt-Martin, G. D. Stucky and F. Schüth, *Science*, 1996, **273**, 768.
6 G. Fornasieri, S. Badaire, R. Backov, O. Mondain-Monval, C. Zakri and P. Poulin, *Adv. Mater.*, 2004, **16**, 1094.
7 V. N. Manoharan, A. Imhof, J. D. Thorne and D. J. Pine, *Adv. Mater.*, 2001, **13**, 447.
8 F. Carn, A. Colin, M.-F. Achard, H. Deleuze and R. Backov, *Adv. Mater.*, 2004, **16**, 140.
9 F. Carn, N. Steunou, A. Colin, J. Livage and R. Backov, *Chem. Mater.*, 2005, **17**, 644.
10 F. Carn, A. Colin, M.-F. Achard, H. Deleuze, C. Sanchez and R. Backov, *Adv. Mater.*, 2005, **17**, 62.
11 A. Clearfield and J. A. Stynes, *J. Inorg. Nucl. Chem.*, 1964, **26**, 117.
12 S. M. Kuznicki, K. A. Trush, F. M. Allen, S. M. Levine, M. M. Hamil, D. T. Hayhurst and M. Mansour, in *Molecular Sieves Synthesis of Microporous Materials*, M. L. Occelli, H. E. Robson, eds. Van Nostrand–Reinold, New York, 1992, vol. 1, pp. 427.
13 (*a*) A. Clearfield and U. Costantino, in *Comprehensive Supramolecular Chemistry*, ed. G. Alberti, T. Bein, Pergamon, Oxford, New York, Tokyo, 1996, vol. 7, pp. 107; (*b*) G. Alberti, M. Casciola, U. Costantino and R. Vivani, *Adv. Mater*, 1996, **8**, 291; (*c*) G. Alberti, M. G. Bernasconi, U. Costantino and J. S. Gill, *J. Chromatogr.*, 1977, **132**, 477.
14 A. A. Marti and J. L. Colón, *Inorg. Chem.*, 2003, **42**, 2830.
15 A. Clearfield, in *Comprehensive Supramolecular Chemistry, Solid-state Supramolecular Chemistry: Two- and Three-dimensional Inorganic Networks*, eds. G. Alberti, T. Bein, Pergamon, New York, 1996, vol. 7 (and references within).
16 V. C. Kumar and A. Chauldari, *J. Am. Chem. Soc.*, 2000, **122**, 830.
17 (*a*) R. Krishnamoorti, R. A. Vaia and E. Giannelis, *Chem. Mater.*, 1996, **8**, 1728; (*b*) J. P. Lemmon and M. M. Lerner, *Chem. Mater.*, 1994, **6**, 207; (*c*) H.-L. Tsai, J. Heising, J. L. Schindler, C. R. Kannewurf and M. G. Kanatzidis, *Chem. Mater.*, 1997, **9**, 879; (*d*) H.-L. Tsai, J. L. Schindler, C. R. Kannewurf and M. G. Kanatzidis, *Chem. Mater.*, 1997, **9**, 875.
18 K. M. Parida, B. B. Sahu and D. P. Das, *J. Colloid Interface Sci.*, 2004, **270**, 436.
19 (*a*) J. Fricke, in *Aerogels*, Springer-Verlag, Berlin, 1986; (*b*) M. S. Ahmed and Y. A. Attia, *Appl. Therm. Eng.*, 1998, **18**, 787; (*c*) A. Khaleel, P. N. Kapoor and J. J. Klabunde, *NanoStruct. Mater.*, 1999, **11**, 459; (*d*) S. Yoda, K. Ohtake, Y. Takebayashi, T. Sugeta and T. Sako, *Mater. Chem.*, 2000, **10**, 2151.
20 D. M. Kas-hak, S. A. Johnson, D. E. Hooks, H.-N. Kim, M. D. Ward and T. E. Mallouk, *J. Am. Chem. Soc.*, 1998, **120**, 10887.
21 (*a*) T. E. Mallouk and J. A. Gavin, *Acc. Chem. Res.*, 1998, **31**, 209; (*b*) E. Brunet, M. Huelva and J. C. Rodriguez-Ubis, *Tetrahedron Lett.*, 1994, **35**, 8697; (*c*) G. Alberti, U. Costantino, C. Dionigi, S. Murcia-Mascaros and R. Vivani, *Supramol. Chem.*, 1995, **6**, 29; (*d*) G. Alberti, L. Boccali, C. Dionigi, R. Vivani, V. I. Kalchenko and L. I. Atamas, *Supramol. Chem.*, 1996, **7**, 129; (*e*) E. Brunet, M. Huelva, R. Vazquez, J. Olga and J. C. Rodriguez-Ubis, *Chem.-Eur. J.*, 1996, **2**, 1578; (*f*) B. Zhang and A. Clearfield, *J. Am. Chem. Soc.*, 1997, **119**, 2751; (*g*) R. Backov, D. J. Jones, B. Bonnet and J. Roziere, *Chem. Mater.*, 1997, **9**, 1812.
22 (*a*) S. W. Keller, H.-N. Kim and T. E. Mallouk, *J. Am. Chem. Soc.*, 1994, **116**, 8817; (*b*) D. M. Kaschak and T. E. Mallouk, *J. Am. Chem. Soc.*, 1996, **118**, 4222; (*c*) M. Fang, D. M. Kaschak, A. C. Sutorik and T. E. Mallouk, *J. Am. Chem. Soc.*, 1997, **119**, 12184.
23 (*a*) G. Alberti, M. Casciola and U. Costantino, *J. Colloid Interface Sci.*, 1985, **107**, 256; (*b*) G. Alberti, M. Casciola, U. Costantino and F. Di Gregorio, *Solid State Ionics*, 1989, **32/33**, 40; (*c*) G. Alberti, M. Casciola and R. Palombari, *Solid State Ionics*, 1993, **61**, 241.
24 (*a*) A. Clearfield and R. M. Tindwa, *J. Inorg. Nucl. Chem.*, 1979, **41**, 871; (*b*) R. M. Tindwa, D. K. Ellis, G.-Z. Peng and A. Clearfield, *J. Chem. Soc., Faraday Trans. 1*, 1985, **81**, 545; (*c*) J. Xu, Y. Tang, H. Zhang and Z. Gao, *J. Inclusion Phenom. Mol. Recognit. Chem.*, 1997, **27**, 303.
25 G. Alberti and E. Torraca, *J. Inorg. Nucl. Chem.*, 1968, **30**, 317.
26 R. Phelan, D. Weaire, E. A. J. F. Peters and G. Verbist, *J. Phys.: Condens. Matter*, 1996, **8**, 475.
27 D. Exerowa and P. M. Kruglyakov, in *Foams and Foam Films Theory, Experiment, Application*, eds. D. Möbius, R. Miller, Elsevier, Amsterdam, 1998, vol. 5.